DOI 10.1007/s10553-021-01235-w
*Chemistry and Technology of Fuels and Oils, Vol.57, No.1, March, 2021 (Russian Original No.1, January – February, 2021)*

# A STUDY ON CHARACTERISTICS OF UNSATURATED SANDY SOILS BASED ON THE CT SCANNING METHOD

**Tian Zhao[1,2,3], Xian-chun Tang[1,2*], Gui-ling Wang[1,2], Li Wan[3], Xu-sheng Wang[3], and Xin-xinZhang[1,2]**

*In the hydrologic cycle, sandy soils play the role of a connecting reservoir of surface water and groundwater, particularly in arid areas. Therefore, to provide water conservation and ecological environment protection, it is important to study the soil water behavior in the unsaturated zone. At present, the CT-scan method is commonly used to study the soil hydraulic properties. In the field of materials science, the industrial CT high-resolution instruments are applied for quantitative research on the porous microstructure and fluid filtration law in sandy soils.*

*In this study, we have studied five samples of sand scans of the quartz sand and CUGB coarse sand types. The industrial-type CT instrument XTH225ST was used for the sample microstructure scanning. In order to identify water, air, and solid particle distribution of the sample cross section, and to analyze the particle size distribution and moisture content, the scanned images were processed using the VG-Studio and ImageJ software.*

*Comparing the CT-scan results of the four quartz sand samples, it can be concluded that the optimal particle size ranges from 1 to 2 mm. According to the porosity quantitative analysis, with decrease in the particle size, the total porosity of the soil sample increases. After applying the image recognition*

[1]Chinese Academy of Geological Sciences,China Geological Survey, Ministry of Natural Resources, Beijing 100037, China. [2]SinoProbe Center, Chinese Academy of Geological Sciences, China Geological Survey, Ministry of Natural Resources, Beijing 100037, China. [3]China University of Geosciences, Beijing 100083, China. *Corresponding author: Xian-chun Tang. E-mail: tangxianchun@cags.ac.cn.* Translated from *Khimiya i Tekhnologiya Topliv i Masel*, No. 1, pp. 92 – 96, January – February, 2021.

 

*and VG- Studio software, we can see that for different particle sizes of the sand sample, the average pore size increases with increase in the particle size.*

*To study the moisture absorption and desorption phenomenon, two samples of the CUGB coarse sand are experimentally studied. The particle size of the samples ranges from 1 to 2 mm. The CT scanning analysis is used to obtain the unsaturated characteristic curve of the soil when the moisture content reaches stability. Due to the lag phenomenon, the characteristic curve of the soil moisture has an obvious "loop," or hysteresis, shape. As shown by a 3D modeling, the distribution of capillary water in the sand column is complex, and the water flow forms multiple winding paths, like "worms" creeping in the soil.*

*The CT-scan method is used to overcome the limitations of the traditional experimental methods and to evaluate the relationship between the moisture content and the matrix suction. The obtained characteristic curve of soil moisture can be used to improve the efficiency of technological operations. The CT-scan method provides a new way of evaluating the water distribution characteristics of unsaturated soils.*

***Keywords:*** *CT-scan, capillary water, porosity, characteristic curve of soil moisture.*

## 1 INTRODUCTION

Groundwater flows in the pores or fractured channels of the water-containing medium. The microstructure of pores and cracks determines the hydrogeological properties of the water-bearing medium. When the water-containing medium is in an unsaturated state, the pores and cracks are not only filled with capillary water but also with air. As a result, the medium is a three-phase structure consisting of solid, liquid, and gaseous phases. The study of the water characteristics in the unsaturated zone is of great significance for the ecological environment and soil-water conservation. At present, two types of methods are widely used for determining the relevant moisture characteristic curves of sands. One is the direct test, and the other is the indirect estimation method.

The first type is based on experimental measurements of the negative pressure and moisture content of the sample in different states, and the empirical formulas are used for calculations. The traditional methods include a negative pressure gauge method, sand funnel method, and tensiometer method [1-3]. Other techniques of measuring the moisture content of sands include the drying method, the neutron method, and TDR (time-domain reflectometry) method [4-6]. This type of testing methods is relatively clear in concept, and the experimental conditions and operations are controllable. Therefore, it is commonly used to determine the moisture characteristic curve of sand. On the other hand, the above methods can be time-consuming, labor-intensive, and capital-consuming, and the measurement range is limited. The sand moisture characteristic curve cannot be obtained within the entire moisture content range. The other type is the indirect derivation type. It includes such methods as the sand conversion function method, the fractal theory, and the sand morphology method [7-10]. Industrial CT scanning is mainly applied with the sand morphology and fractal method, and it can be also used with empirical formulas for exploration and research.

The basic idea of the sand morphology method is to determine the pore size distribution and connectivity of sand through the analysis and processing of a series of high-resolution sand profile images, and to build a mesh model. Firstly, some researchers proposed to use a network model to study the relationship between the hydraulic properties and the void structure of sand [11]. Many scholars have also made useful suggestions on the application of network models in sand physics and groundwater hydrology. For example, a network model was used to study the moisture characteristic curve, which more accurately reflects the void size distribution

law, and the results were compared with the real situation to verify the reliability of the network model [12-15]. In essence, using morphological theories to analyze the relevant hydrological properties of sand can provide reliable and accurate results, but the methods are cumbersome and difficult to operate in real situations.

In recent years, the application of industrial CT instruments has been introduced into the study of sand hydrodynamics. For the first step, a special CT scanner was used to obtain a series of color images of sand and soil [16-20]. The CT scanning technology was used to observe the phenomenon of capillary water flow in fractures. As shown by CT scanning, the hydrostatic pressure gradient causes the vertical uneven distribution of water content and water surface tension. Regardless of macro-scale and micro-scale features, the uneven distribution determines the optimal path of capillary water filtration. [21]. The water retention potential of sand is almost equivalent to the capillary water content in fractures. The unsaturated sands have been studied by the regional growth method and industrial CT-scan data, but the method is only accurate for the unsaturated regions with large pores [22]. The X-ray CT scanning technology has been used to study the capillary properties of Nubia sandstone [23]. The analysis of sands with particles of different size and different pore volume allowed the scholars to define a new physical parameter – the typical unit volume (REV) size — and to perform a series of tests of the sand-water properties [24-26]. In this research, the CT scanning method is applied to produce high-precision data images. Summing up, the application of large-scale industrial CT high-resolution instruments to quantitative analysis of the microstructure and fluid flow laws of porous media has become an emerging research focus in the field of geoscience and materials science [27].

## 2 EXPERIMENTAL METHOD AND SAND SAMPLE TREATMENT

The instrument used in this test is the XTH225ST scanner produced by Nikon. The scanner is used for nondestructive detection of the two-dimensional and three-dimensional structures, with a minimum resolution of 3 $\mu$m.

The XTH225ST scanner characteristics are the following: minimum focus 3 $\mu$m for the launch target, X-ray tube voltage 200 kV, power 40 W, and density resolution 1.27%. The instrument is equipped with three X-ray sources, namely: 225 kV reflective target, 225 kV rotating target, and 180 kV transmission target.

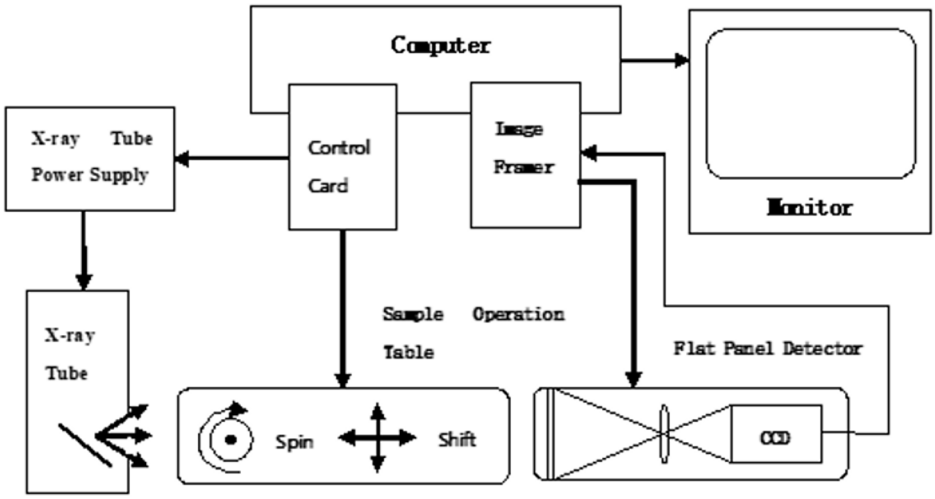


Fig.1. Schematic diagram of the micro-focus CT scanner.

Figure 1 shows the schematic diagram of the micro-focus CT scanner. The cone beam X-ray emitted by the X-ray source passes through the sample and forms a transmission image on the detector. The detector records the image and sends it to the workstation for processing and saving the transmission images.

The principle of large-scale high-resolution industrial CT scanning technology is based on network *coImputer* tomography, or CT technology. When the incident X-ray passes through the sample material, the ray intensity is attenuated by the absorption or scattering of the material along the ray path. The attenuation is determined by Beer's law, and the attenuation coefficient is used to display the attenuation level [28-29]. In general, it can be assumed that for the non-uniform material the attenuation coefficient of this plane is ì(x, y), the incident intensity of the ray is $I_0$, the intensity of the ray after passing through the material is $I$, and the path length of the ray in the sample is $L$. The relationship between $I_0$, $I$, and $\mu$(x, y) is determined by Beer's law and can be expressed as [30]

$$I = I_0 \exp\left[-\int_L \mu(x,y)dxdy\right] \tag{1}$$

where $I$ is the output intensity, $I_0$ is the initial intensity, and $\mu$ is the attenuation coefficient, $m^{-2}$. After simplifying, we obtain

$$\int_L \mu(x,y)dxdy = In\frac{I_0}{I} \tag{2}$$

If the values of I0 and $I$ are evaluated by the detector, then the line integral of the attenuation coefficient ì along the path $L$ can be calculated.

When the incident electron penetrates the surface of the material at a definite angle, the corresponding line integral values of the attenuation coefficient for all paths can be obtained by using the formula, resulting in a set of values. For a infinite set of values, the distribution of the attenuation coefficient of the material surface can be accurately solved.

Some studies have shown that the attenuation coefficient of the sample is mainly related to the mass density and the atomic number of the substance, so the two-dimensional distribution of the attenuation coefficient can also be interpreted in terms of the two-dimensional distribution of density [31]. Besides, the actual ray beam always has a definite cross-section. The principle of radiography can be solved by the finite difference method in space. Previous studies have found that the attenuation coefficient of X-ray is affected by the energy intensity of X-ray photons. The CT number is often used to replace the attenuation coefficient [32]:

$$CT = \frac{1000\times(\mu_i - \mu_w)}{\mu_w} \tag{3}$$

where $CT$ is the CT number of the material, $\mu_i$ is the attenuation coefficient of the material, and $\mu_w$ is the attenuation coefficient of water. The CT number is more stable than the attenuation coefficient and does not change drastically with the incident X-ray photon energy variation.

The industrial CT-scan instruments produce images in TIFF data format. The original image is similar to that of a hospital X-ray film. In order to identify the microstructure, the original images need to be further

processed by the computer software. In this study, the VG Studio software is used to process and output the original pictures obtained by X-ray CT scanning.

In the study of sand solid particles, the materials with different densities have different gray image values. In general, the pores on the CT image are black when they are filled with air, and the solid particles are generally gray-white, as shown in Figs. 2 - 6. Within the gray range of 0-255, one of the peaks corresponds to the gray value of the pore, and the other represents the gray value of the particles. To distinguish the air in the pore from the sand, we need to select the appropriate gray-scale threshold. As the density of air is lower than that of the solid material, a gray value of air is smaller. The complete left wave peak represents the pores. On the contrary, the density of sand particles is higher, and the color of the CT-scan image is white. Therefore, the complete peak on the right represents sand particles. The main factors influencing the gray threshold include threshold method, image parameters, the influence of experimental operations, and so on.

Generally, to provide the image binarization and threshold segmentation, a function module needs to be transferred to convert the original image into a gray-scale image, calculate the gray-scale distribution frequency map, perform threshold segmentation, and divide the solid particle, water, and gas three-phase boundaries. Based on the MATLAB platform, the author programmed the water-gas-solid three-phase recognition software of CT-scan images. A comparison with VG Studio and ImageJ software showed that the developed software can satisfactorily identify the water-gas-solid phase boundaries.

As for the sand sample treatment, the large-scale high-resolution industrial CT-scan experiment of the sand pore structure is divided into two major stages. In the first stage, the samples of the quartz sand with different particle sizes were selected for the CT scanning test, and the preliminary experiments were carried out. The particle size of the four sand samples varied in the range 0.25-0.5, 0.5-1, 1-2, and 2-4 mm. To obtain the optimal observation diameter of the sand pore structure, quartz sand was selected as the material for the first phase of the experiment. The quartz sand is produced by crushing quartz stone. It has a hard texture and stable chemical composition, similar to the real sand. It is an ideal experimental material to simulate the real sand in the tests of the pore structure.

In the second stage, the CUGB coarse sand was selected for testing. Coarse sand is a trough sand material supplied by the Hydraulic Engineering Laboratory, China University of Geosciences, Beijing. Coarse sand was used for the study of the three-dimensional shape of the water-pore structure in the sand. The CUGB sand has good continuity, poor gradation, distinct edges, and corners; it does not contain powder and clay particles and belongs to a coarse sand type.

Through the laboratory tests, it is determined that the specific gravity of the CUGB coarse sand is 2.66 g/cm$^3$, the porosity is 0.41, and the saturated permeability coefficient is 166.92 m/d. It is an ideal test sample representing the real sand material. Therefore, it was selected to study the three-dimensional microscopic morphology of the pores. A further screening experiment was carried out on the CUGB coarse sand, and according to the result of the first stage CT scanning, particles of 1.0-2.0 mm were selected. Two identical organic glass test tubes were used, the inner diameter was 45 mm, outer diameter 50 mm, and overall height 155 mm. The two test tubes were connected with a rubber tube to form a U-shape tube system. The rubber tube was equipped with a water stop clamp. The left test tube was filled with CUGB coarse sand, and the right test tube was filled with deionized water that eliminated the interference of impurities in the water.

## 3. SCANNING ANALYSIS OF SAND PORE STRUCTURE

The structure of many natural substances consists of pores and cracks that define the fundamental properties of the substances. In the natural state, the main characteristic of the pore structure is the porosity, which refers to the percentage of the volume of pores in a porous medium to the entire volume of the medium:

$$P = \frac{V - V_0}{V} \times 100\% \tag{4}$$

where $P$ is the porosity, %; $V$ is the total volume, also called the apparent volume, mm$^3$; and $V_0$ is the volume occupied by solid particles, mm$^3$.

The porosity can be divided into total porosity (namely, absolute porosity) and effective porosity. The porous medium may contain tiny pores that are not connected with each other. The absolute porosity is the ratio of the total volume of all pores in the volume and the outer surface of the porous medium. The effective porosity is the percentage of the total volume of interconnected pores in the porous medium to the total volume of the sample.

The CT scanning technology allows to identify the tiny pores that are not interconnected. As long as the results calculated by the VG Studio software include pores that are not connected to each other, the obtained porosity is the absolute, or total, porosity.

After scanning the four sand samples, it can be concluded that the CT-scan cross-sections of the two types of quartz sand columns contained particles with diameters of 0.25-0.5 and 0.5-1 mm, respectively, the particle distribution is dense, and the resolution is not high. It is difficult to distinguish the phase boundaries between solid particles, water, and gas phases by the naked eye, and computer recognition is even more difficult, resulting in increasing error of computer calculations of the cross-sectional porosity. For the 2-4 mm quartz sand, the particle size is large, the pores are also large, and the deviation from the real values is significant. If the cross-sectional porosity is obtained by this method, the increase in the calculated porosity value will cause an increase in error. For the XTH225ST large-scale CT scanner, it is more reasonable that the change characteristics of the cross-sectional porosity and the three-dimensional distribution of capillary water of the sand column are explored by choosing samples with 1-2 mm particle size. Such samples can provide higher resolution and smaller calculation errors.

The transmission phenomenon module in VG Studio software can be used to solve the trend of porosity changes with height. The abscissa of the graph of the sample porosity versus height represents the position of the cross surface, the bottom of the sample is recorded as the zero point of the cross surface, and the value represents the height of the sample. With increase in the sample height, the porosity slightly and gradually decreases. This means that the porosity at the bottom is larger and the porosity at the top is smaller. In the change graph, the experimental results of the 0.5-1 mm quartz sand sample are particularly obvious. In addition, the results are also analyzed and calculated.

a) The total porosity of the quartz sand sample with a particle size of 2-4 mm is 43.6%. As shown in Fig. 2, the line represents the changing trend of porosity with height. In general, the porosity exhibits an “electrocardiogram” vibrating type of distribution around 43.6%, and the amplitude is comparatively large. It can be seen that the porosity of the adjacent cross-section of quartz sand with a particle size of 2-4 mm varies greatly, in the range between 39.8% and 50.5%.

b) The total porosity of the quartz sand sample with a particle size of 1-2 mm is 45.3%, and the overall porosity is around 45.3% in an “electrocardiogram” vibrating-type distribution, but the vibration amplitude is

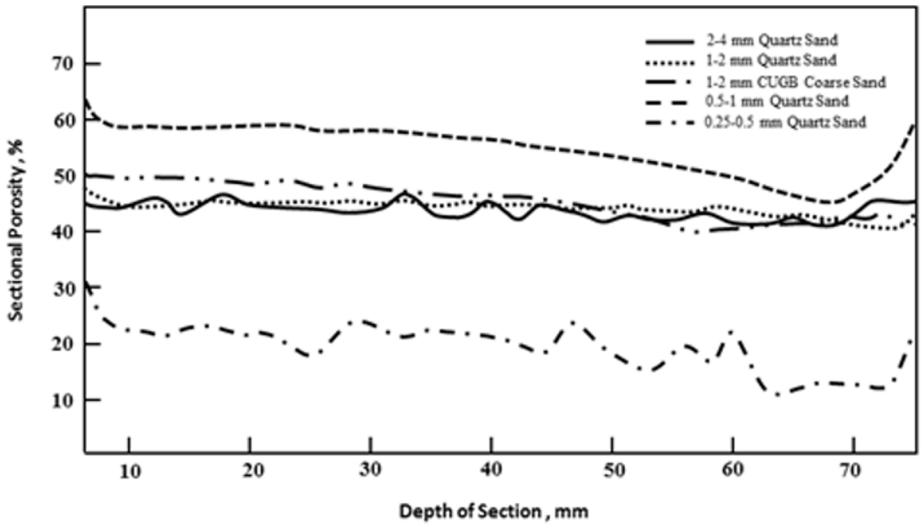


Fig.2. The tendency graph of porosity with the depth of section.

similar to that of the quartz sand test with 2-4 mm. The sample is relatively small, fluctuating in the range of 41.2%-48.6%. The degree of porosity changing in adjacent cross-sections is smaller.

c) The total porosity of the quartz sand sample with a particle size of 0.5-1 mm is 54.8%. In general, the porosity is larger on the bottom and smaller on the top. This shows a small vibration-type distribution that fluctuates in the range of 42.8%-61.5%. The vibration amplitude is smaller than that of 2-4 mm and 1-2 mm quartz sand samples.

d) The total porosity of the quartz sand sample with a particle size of 0.25-0.5 mm is 20.3%. In general, the porosity fluctuates significantly and the error is high. The resulting curve shows a significant deviation. The reason may be due to the small size of the sample. The VG Studio software is used to recognize the interface between solid particles and air on the CT-scan cross-section image. Therefore, the accuracy of recognition is reduced and the resulting curve does not show a clear uniform law.

e) For the 1-2 mm coarse sand samples, the above experimental procedures were repeated to obtain the porosity change graph of the coarse sand material with height, as shown in Fig.2. In general, the porosity of the CUGB coarse sand exhibits an “electrocardiogram” vibration-type distribution around 43.1% and fluctuates slightly in the range of 39.8%-50.9%. The results confirm the earlier conclusions: For the same sand column, the porosity decreases gradually with increase in height.

In summary, when the particle size decreases, the overall volumetric porosity of the sand increases, and the range of porosity changing at adjacent heights also decreases. For the same sand column, the porosity at the bottom is slightly larger than that at the top, that is, as the height increases, the porosity will gradually decrease.

The average porosity of the coarse sand sample obtained by CT scanning is 43.1%, which is similar to the porosity of the 1-2 mm quartz sand sample, which is 45.3%. The results show that different porous media with the same particle size demonstrate the same porosity values. The measured porosity of the CUGB coarse sand is 41%. After calculation, the experimental porosity error is within 5%, proving that the accuracy is high.

## 4 SCANNING ANALYSIS OF MOISTURE CHARACTERISTICS OF UNSATURATED SAND

After CT scanning of the four sand columns, we obtained four sets of images containing 2049, 2289, 2168, and 2189 cross-sectional views of the area of interest, respectively.

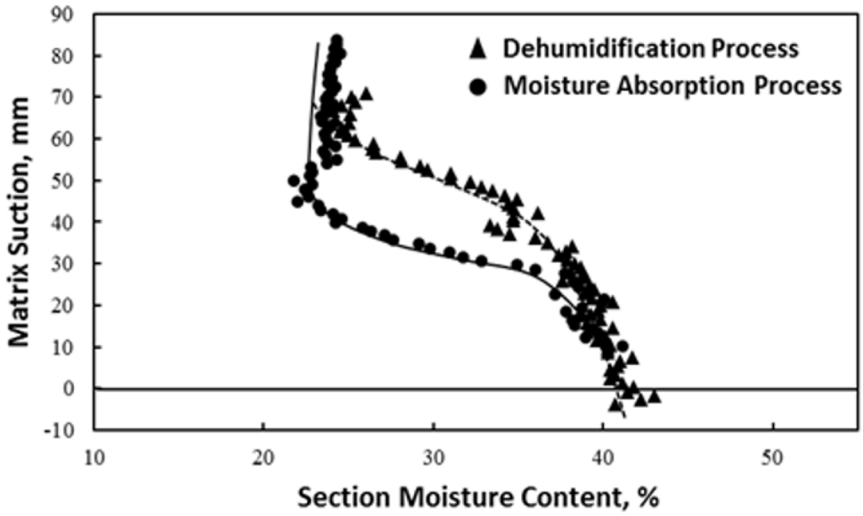


Fig.3. Soil moisture characteristic curve in the process of moisture absorption and dehumidification.

ImageJ and VG Studio software was applied to identify water, solid particles, and air, and then the water content of every cross-section was calculated. Calculating the moisture content of all sections of the sand column can characterize the change of the moisture content with height. Based on the calculation results, the moisture characteristic curve can be plotted. In the experiment, the pressure head is assumed as the negative value of the height relative the water level in a static state. In soil hydrodynamics, matrix suction is often used to express the pressure head of capillary water. Therefore, the suction force of the matrix is the same value as the height of the corresponding water level in this experiment. The same method is applied to process all data images of the dehumidification and moisture absorption process. The resulting moisture characteristic curve of the moisture absorption and dehumidification process of the big coarse sand is shown in Fig. 3.

The soil moisture characteristic curve represents the relationship between water content and substrate suction. The moisture characteristic curves are widely used in soil dynamics. With the CT scanning method, the relationship between water content and matrix suction can be directly calculated, improving the efficiency.

As shown in Fig. 3, the soil moisture characteristic curve demonstrates the hysteresis phenomenon, also known as the principle of meniscus delay formation or contact angle theory. When the temperature is constant and consistent, the characteristic curve shows different moisture content figures of the absorption process and dehumidification process. The curve's endings are approximately coincident, and the loop is formed in the middle, as shown in Fig. 3.

According to the soil moisture characteristic curve in Fig.3, it can be concluded that the saturated water content $\theta_S$ is 42%, the air intake is 32 mm, and the residual water content is 21%. The saturated water content is basically consistent with the porosity of the large and coarse sand, indicating that the saturated water content has a higher accuracy. However, the residual moisture content deviates significantly from the actual level, as the reasonable range of the residual moisture content, evaluated by other methods, should be 5%-7%. When the images were processed by the software, a thin film of water film on the edges of the solid particles was also recognized and included in the moisture content calculation; hence the resulting residual moisture content was higher than the normal value.

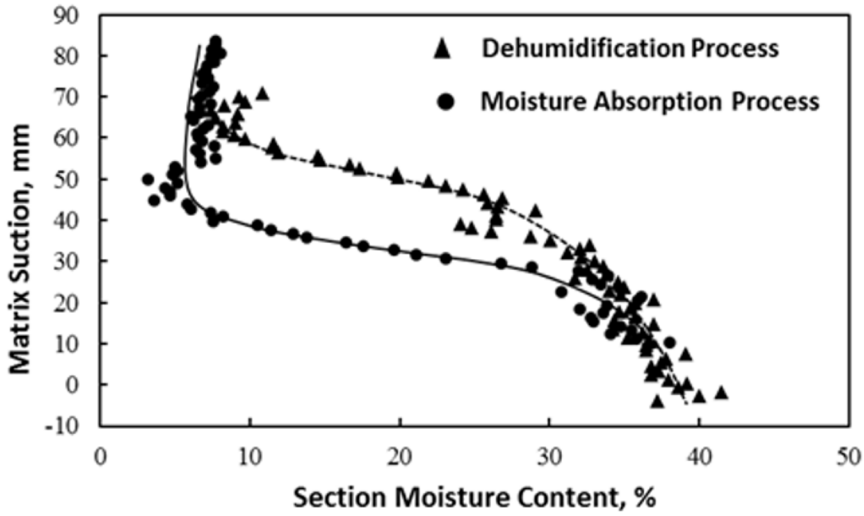


Fig. 4. The corrected soil moisture characteristic curve of absorption and dehumidification.

Based on the soil moisture characteristic curve, the corrected cross-section moisture content is calculated as

$$Q_{cor} = \frac{Q - Q_{\min}}{Q_{\max} - Q_{\min}} \left( Q'_{\max} - Q'_{\min} \right) \tag{5}$$

where $Q_{cor}$ is the corrected cross-sectional water content, %; $Q$ is the software-processed water content of a cross-section, %; $Q_{\min}$ is the minimum cross-sectional water content, %, $Q_{\min}$ is 21%; $Q_{\max}$ is the maximum water content identified by software, %, (%), $Q_{\max}$ is 42%; $Q'_{\min}$ is the minimum true value of the cross-sectional water content, which is taken as 5% according to previous experimental results; and $Q'_{\max}$ is the maximum true value of the cross-sectional water content, the value of which is the same as the maximum value of the cross-sectional water content recognized by the software.

Substituting the values in Eqs. (5) and (6), we obtain

$$Q_{cor} = \left( Q - 21 \right) \times 1.8 \tag{6}$$

Figure 4 shows the corrected characteristic curve of the moisture absorption and dehumidification process. After correction, the residual moisture content is 4.8%, which is consistent with the earlier research results.

Using VG-Studio software, the capillary water suction and profile morphological characteristics can be clearly and intuitively obtained by the CT scanning data. Using the VG-Studio and ImageJ software, the cross-sectional CT map can be used to identify the water content and to obtain the capillary water distribution map, which is conducive for analysis and calculation. Considering the morphology of samples, the CT images show that the capillary water fills the pores and forms almost circular bubbles. The pores are circular in shape and are unevenly distributed in the sand column. The capillary water is more densely distributed in the center and sparsely distributed on the edges. The capillary water surrounds the edges of the solid particles, forming

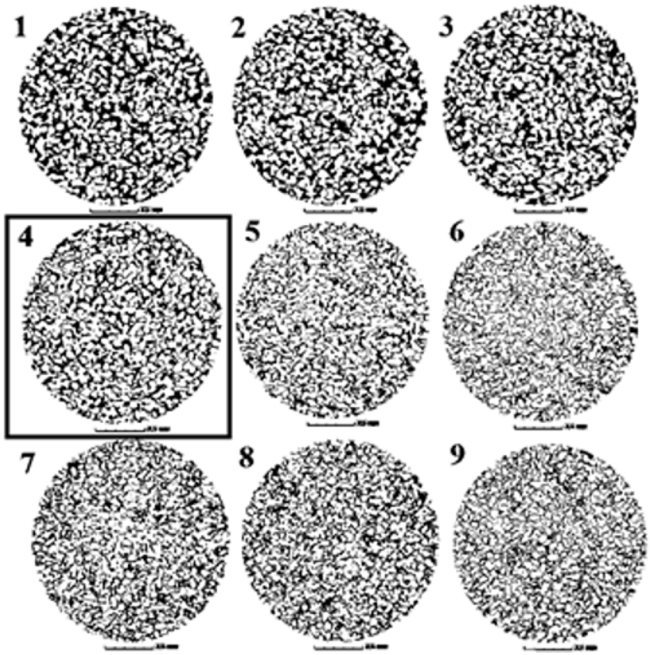


Fig.5. Cross-sectional ratio of capillary water at different heights of coarse sand column.

a thin water film. The capillary water flow is complicated. Water upward flow overcomes the potential energy of the soil matrix. Water can adhere to solid particles under the combined action of adsorption on the particle surface and the capillary effect between the particles.

To evaluate the adsorption and capillary effect of the soil matrix, we have compared the cross sections of the sample when the water height level ranges from -30 to 50 mm, as shown in Fig. 5. The cross sections corresponding to the water height level are numbered from 1 to 9. Figure 5 shows a cross-sectional ratio diagram of capillary water at different positions of the sample sand column. The diagram represents the change in the pore water distribution from the bottom to the top of the test tube. It can be concluded that the closer the U-shaped tube to the reference liquid level, the greater the proportion of the dark areas corresponding to the capillary water content at different levels.

It can be concluded from Fig. 5 that the cross-section No. 4 shows the most obvious change of isometric structure among all images, from the bottom to the top of the sand column surface. This may correspond to the position of the water surface, which reflects the water level of the U-shaped pipe. The water surface acts as the interface; thus, the capillary water occurs over the interface, and the saturated water occurs below the interface.

The form of the capillary water flow path is complicated and determined by a number of factors. As shown in Fig. 6, the capillary water path in the longitudinal cross-section is characterized by irregular distribution. The capillary water at the bottom fills most of the pores and continues to rise under the combined action of adsorption and capillary effect. The capillary water is distributed intermittently near the tube wall. In the center of the tube, the degree of water filling the pores is higher, the hydraulic connection between the pores is better developed, and the capillary water rising path is tortuous and complicated. As shown in Fig. 6, the distribution of capillary water is intricately intertwined like a net in the sand column, and the path is winding like a crawling route of “earthworms.” In general, the net is better developed around the edges of the solid particles, but some particles are not surrounded by the capillary water. The capillary water upward flow path is also affected by such factors as the sand particle size, properties of solid particles, temperature, and fluid characteristics.

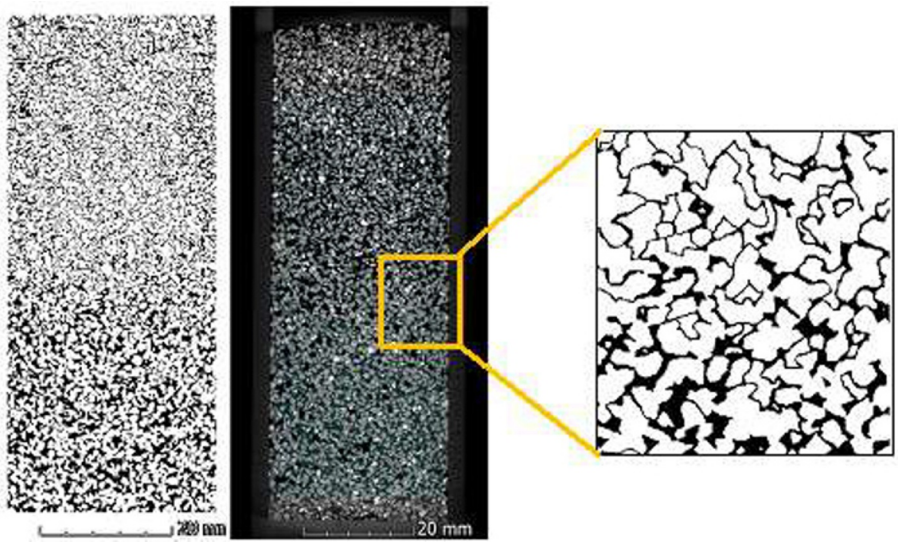


Fig. 6. Diagram of the upward flow path of capillary water.

## 5 CONCLUSIONS

This paper focuses on the study and analysis of sand pore structure, unsaturated sand-water characteristics, and three-dimensional morphology of sands with different particle sizes of quartz sand and CUGB coarse sand by using the latest industrial CT scanner XTH225ST. The following conclusions can be drawn.

1. It can be seen that the total porosity of the sand sample increases with decrease in the particle size. The range of the porosity variations of the adjacent cross-section heights also decreases. With increase in height, the porosity gradually decreases.

2. Comparing the sand sample columns of different particle sizes, it can be seen that with increase in particle size, the average pore diameter also increases.

3. The CT scanning method is used for direct calculation of the relationship between moisture content and matrix suction and obtaining the soil moisture characteristic curve. The curve reflects an obvious hysteresis effect.

4. The pattern of capillary water distribution in the sand column is similar to a three-dimensional net, which is intricately intertwined, and the path is meandering like an “earthworm.” For the longitudinal cross section, the capillary water is unevenly distributed inside the sand sample. For example, water is densely distributed in the center part of the tube and sparsely distributed on the edges, forming a thin water film around the solid particles.

5. The capillary water shows a irregular distribution in the longitudinal section. At the bottom, the capillary water fills most of the pores. Moreover, the capillary water continues to rise under the combined action of adsorption and capillary effect. Near the tube wall, the capillary water is distributed intermittently. In the center of the tube, the degree of water filling the pores is higher, the hydraulic connection between the pores is better developed, and the capillary water rising path is tortuous and complicated.

**ACKNOWLEDGMENTS**

*This work was financially supported by the Basic Scientific Research CAGS (No. JKY201901-04, No. JYYWF20181101, and JKY202007), Geological Survey Projects of China Geological Survey (No.DD20190132), and the National Natural Science Fund Project (41877197 and 41602257).*

**REFERENCES**

1. J. R. Wang and T. J. Schmugge. "An empirical model for the complex dielectric permittivity of soils as a function of water content," *IEEE Trans. Geosci. Rem. Sens.*, 4, 288-295 (1980).
2. D. Croney and J. D. Coleman, *Pore Pressure and Suction in Soil*, Butterworths, London (1961).
3. J. Lipiec et al., "Measurement of plant water use under controlled soil moisture conditions by the negative pressure water circulation technique," *Soil Sci. Plant Nutr.*, 34(3), 417-428 (1988).
4. M. K. Krokida and Z. B. Maroulis, "Effect of drying method on shrinkage and porosity," *Drying Technol.*, 15(10), 2441-2458 (1997).
5. J. Ledieu et al., "A method of measuring soil moisture by time-domain reflectometry," *J. Hydrol.*, 88(3-4), 319-328 (1986).
6. J. D. Tandy and M. Visvalingam, "The neutron method for measuring soil moisture content-a review," *J. Soil Sci.*, 23(4), 499-511 (1972).
7. M. Rieu and G. Sposito, "Fractal fragmentation, soil porosity, and soil water properties: I. Theory," *Soil Sci. Soc. Am. J.*, 55(5), 1231-1238 (1991).
8. T. C. Lippmann and R. A. Holman, "The spatial and temporal variability of sand bar morphology," *J. Geophys. Res.: Oceans*, 95(C7), 11575-11590(1990).
9. D. J. Disraeli, "The effect of sand deposits on the growth and morphology of *Ammophila breviligulata*," *J. Ecol.*, 72(1),145-154 (1984).
10. E. Y. Lee et al., "Effects of gelatinization and moisture content of extruded starch pellets on morphology and physical properties of microwave-expanded products," *Cereal Chem.,* 77(6), 769-773 (2000).
11. I. Fatt, "The network model of porous media," *Trans. AIME*, 207(01), 144-181(1956).
12. R. P. Ewing and S. C. Gupta, "Modeling percolation properties of random media using a domain network," *Water Resour. Res.*, 29(9), 3169-3178 (1993).
13. G. S. Campell, "A simple method for determining unsaturated hydraulic conductivity from moisture retention data," *Soil Sci.*, 117, 311-314 (1974).
14. Y. Mualem, "A new model for predicting the hydraulic conductivity of unsaturated porous media," *Water Resour. Res.*, 12, 513-522 (1976).
15. R. Van Genuchten, "Predicting the hydraulic conductivity of unsaturated soils," *Soil Sci. Soc.*, 44, 892-898 (1980).
16. K. Roth, H. J. Vogel, and R. Kasteel, "The scaleway: A conceptual framework for upscaling soil properties," *Model. Trans. Proc. Soils*, 1, 24-26 (1999).
17. M. Cyìslerova and J. Votrubova "CT derived porosity distribution and flow domains," *J. Hydrol.*, 267(3), 186-200 (2002).
18. A. Garbout, L. J. Munkholm, and S. B. Hansen, "Temporal dynamics for soil aggregates determined using X-ray CT scanning," *Geoderma*, 204–205(4), 15-22 (2013).
19. A. Garbout et al., "Tillage effects on topsoil structural quality assessed using X-ray CT, soil cores and visual soil evaluation," *Soil Tillage Res.*, 128, 104-109 (2013).

20. K. N. Manahiloh and C. L. Meehan, “Determining the soil water characteristic curve and interfacial contact angle from microstructural analysis of X-ray CT images,” *J. Geotech. Geoenviron. Eng.*, 143(8), 04017034 (2017).
21. K. Beven et al., “Macropores and water flow in soils,” *Water Resour. Res.*, 18(5), 1311-1325 (1982).
22. R. H. Brooks and A. T. Corey, *Hydraulic Properties of Porous Media*, Colorado State University, USA (1964).
23. J. F. Bruchon et al., “Full 3D investigation and characterization of capillary collapse of a loose unsaturated sand using X-ray CT,” *Gran. Matter*, 15(6), 783-800. (2013):
24. Y. Higo et al., “Trinarization of ìX-ray CT images of partially saturated sand at different water-retention states using a region growing method,” *Nucl. Instrum. Methods Phys. Res.*, 324, 63-69 (2014).
25. B. S. Nabawy and C. David, “X-Ray CT scanning imaging for the Nubia sandstone as a tool for characterizing its capillary properties,” *Geosci. J.*, 20(5), 691-704 (2016).
26. T. Mukunoki et al., “X-ray CT analysis of pore structure in sand,” *Solid Earth,* 7(3), 929-942 (2016).
27. T. Mukunoki, N. Kumano, et al., “Image analysis of soil failure on defective underground pipe due to cyclic water supply and drainage using X-ray CT,” *Front. Struct. Civ. Eng.*, 6(2), 85-100 (2012).
28. Z. Otwinowski and W. Minor, “Processing of X-ray diffraction data collected in oscillation mode,” *Methods Enzymol.*, 276(97), 307-326 (1997).
29. M. Paradelo, S. Katuwal, P. Moldrup, et al., “X-ray CT-derived soil characteristics explain varying air, water, and solute transport properties across a Loamy Field,” *Vadose Zone J.*, 15(4), 1-13 (2016).
30. R. L. Peyton, C. J. Gantzer, S. H. Anderson, et al., “Fractal dimension to describe soil macropore structure using X ray computed tomography,” *Water Resour. Res.*, 30(3), 691–700 (1994).
31. H. J. Vogel and K. Roth, “A new approach for determining effective soil hydraulic functions,” *Eur. J. Soil Sci.*, 49, 547-556 (1998).
32. W. Tollner and B. P. Verma, “X-ray CT for quantifying water content at points within a soil body,” *Trans. ASAE*, 32(3), 0901-0905 (1989).